

EPIC-pn Energy Scale for Large Window Mode: long-term CTI and pattern corrections

XMM-SOC-CAL-SRN-0367

Ivan Valtchanov, Michael Smith, Norbert Schartel (ESAC)

March 29, 2019

1 CCF components

Name of CCF	VALDATE	EVALDATE	Blocks changed	CAL version	XSCS flag
EPN_CTI_0049.CCF	2000-01-01T00:00:00		LONG_TERM_CTI	3.240	NO
EPN_CTI_0050.CCF	2000-03-23T05:00:00		COMB_EVT_OFFSET LONG_TERM_CTI COMB_EVT_OFFSET	3.240	NO

2 Changes

The long-term charge-transfer inefficiency (LTCTI) correction is updated with the analysis of EPIC-pn observations in Large Window mode (PN-LW). Previously, the correction was based on Full Frame mode observations of the calibration source (*CalClosed* or CC mode), see [8] for details.

There are too few available CC and AGN observations in PN-LW to allow similar approach as for the PN-SW mode. Instead, we use the fluorescent instrumental Cu K α line at 8.04 keV and derive corrections for each of the 12 CCDs at this energy. The Cu K α line is present in all PN-LW observations, we have selected 69 with total exposure greater than 80 ksec. The good statistics for PN-LW mode at the Cu K α line allowed a comparative analysis of the different events patterns, e.g. single (pattern 0) versus double (patterns 1 to 4). Based on this analysis we have derived energy offsets for each of the 12 CCDs so that the single and double events energies match.

The updated LTCTI corrections and pattern offsets described in this report are valid only for PN-LW mode.

3 Energy Scale for EPIC-pn in Large Window mode

3.1 Sample

There are very few *CalClosed* and suitable AGN observations in PN-LW. The two most recent CC are separated by more than 13 years: the latest one is during revolution 3274 ($t = 17.83$ years), while the previous one is during revolution 885 ($t = 4.78$ years). And there are only a few suitable AGN sources, most of them with noisy Fe K α line. Nevertheless, we followed a similar analysis as in PN-SW and derived the line centroids for Mn K α (for *CalClosed*) and Fe K α (for AGNs). The results are shown in Figure 1. There are hints of systematic offsets, however the large error bars and the scarcity of data make it impossible to derive a confident correction.

In PN-LW we have access to the instrumental fluorescent Cu K α line at 8.04 keV. This line is present in all observations and is available with good signal-to-noise in most of the 12 PN CCDs except for CCDs 1, 4, 7 and 10, where it is only available over a small fraction of the total CCD area. The line was used in a preliminary energy scale analysis for Full Frame mode, presented in [3].

In the following we use all 69 PN-LW mode observations with exposure times greater than 80 ksec. The observations start at XMM-Newton revolution 520 ($t = 2.78$ years) and the final one, at the moment of this analysis, is during revolution 3306 ($t = 18$ years). The target of each

observation is irrelevant for the analysis of the Cu $K\alpha$ line. We do not filter the event lists for any intervals of high background. We have found no correlation of the strength of the Cu $K\alpha$ line and the XMM-Newton radiation monitor background levels.

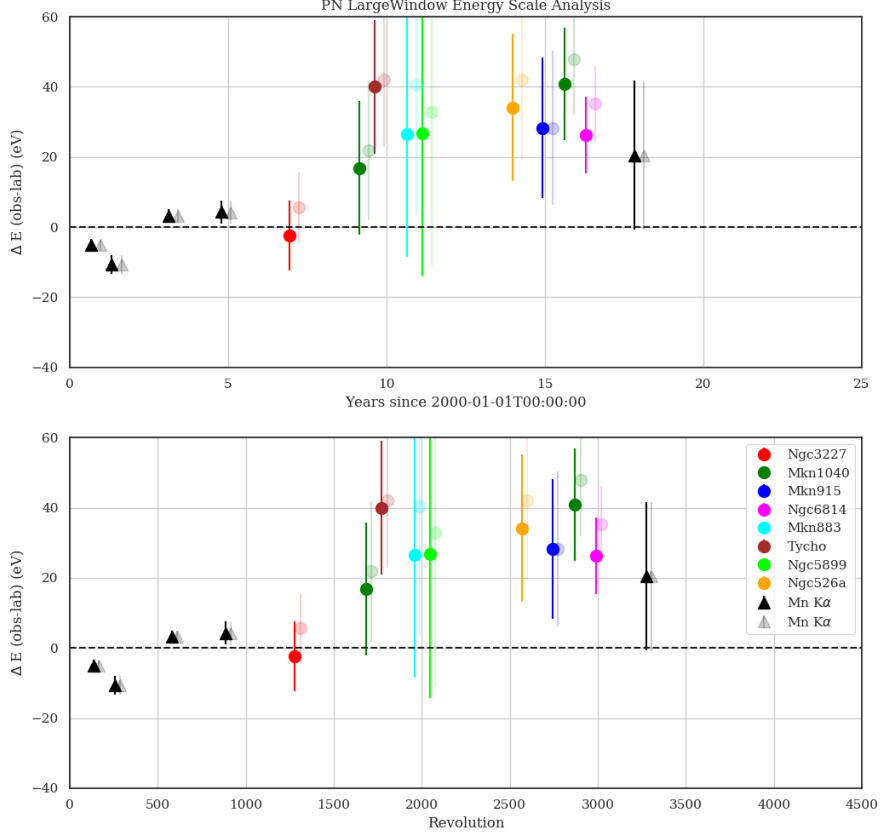


Figure 1: The difference in eV between the observed Mn $K\alpha$ line (CalClosed) energy and for the AGNs the Fe $K\alpha$ line for the available PN observations in Large Window mode. Upper panel is the difference as a function of time (in years since 2000-01-01T00:00:00), the bottom panel is as function of the XMM-Newton revolution. The observations processed with the current calibration (EPN_CTI version 47 and 48) are with semi-transparent symbols; for clarity these are slightly shifted in $+x$ -axis. The darker symbols show the updated results after applying the new correction (see below).

3.2 Processing steps

Initially we process all observations with XMM-SASv17 and the current calibration files. Note that EPN_CTI calibration files are in pairs, the current ones are EPN_CTI_0047 and EPN_CTI_0048. For brevity we are going to refer to those as v48 of the CTI calibration. The steps are similar to those described in [9].

3.2.1 CalClosed

For CalClosed observations we have the following steps:

1. `epchain withctilongterm=Y|N withphagaincolumn=yes propagatecolumns=yes`

2. Extract a spectrum from a box, avoiding the edges, and filter flags and patterns as follows:
`(DETX,DETY) in BOX(517,1430,2500,2250,0) &&`
`FLAG == 0 && PATTERN == 0 && PAT_SEQ == 0`
and we use spectral channels from 0 to 20479.
3. With `specgroup` but no grouping we attach an RMF from the PN-LW canned response matrices and also an ARF from a non CalClosed PN-SW observation. And we set the BACKFILE FITS header keyword to NONE. This is necessary for the next step.
4. Using `XSPEC`, we fit a two-component model (power-law and a Gaussian line), separately for each of the three calibration source lines: Al K_α (1.486 keV), Mn K_α ¹ (5.8988 keV) and Mn K_β (6.490 keV) from the on-board radioactive Iron-55 calibration source. As the source decays, the Mn K_β line is becoming too faint in recent observations and we have not used it in the analysis, although we use it to check the results. The XSPEC fit uses the raw unbinned spectrum.

The observations we use in the analysis are listed in Tab. 2.

3.2.2 Sky sources

The workflow for the sky sources is as follows:

1. `epchain withctlongterm=Y|N`
2. Filtering the event lists with `(#XMMEA_EP && GTI && PI > 150)`.
3. Creating an image in band [2,10] keV and manually define the source and background regions, both circles with radius 640 (32 arcsec).
4. Extract source spectrum and background, using an additional filter with `(FLAG == 0 && PATTERN <= 4)`, and use spectral channels from 0 to 20479 and set `spectralbinsize=5`.
5. Generate an RMF and ARF files.
6. Using `XSPEC`, we fit a simple two-component model (Gaussian line + power-law continuum) limiting the spectral energy range in [4-8] keV. We always keep the line width fixed at 10 eV and set an initial estimate of the line centre at 6.3 keV. Plots of the fit and model to data ratios are shown in Appendix D.

The 8 sky sources we use in the analysis are listed in Tab. 3. Note that we could not identify any more sky sources with narrow Fe $K\alpha$ line and enough signal-to-noise at revolutions greater than 1500.

3.2.3 Cu $K\alpha$ fluorescent line

For the Cu $K\alpha$ analysis we perform the following steps:

1. `epchain withctlongterm=Y|N`.
2. Extract source spectrum from for each of the 12 EPIC-pn CCDs. The good area is selected with mask files, excluding pixels near the edges². The final filtering expression is:
`(PATTERN==0) && (PAT_SEQ==0) && #XMMEA_EP &&`
`mask(maskFile,1,1,RAWX,RAWY) && (CCDNR == ccdnr),`
where `ccdnr` runs from 1 to 12, and we use spectral channels from 0 to 20479 and set `spectralbinsize=5`.

¹What we call Mn K_α is actually a doublet with Mn $K_{\alpha 1}$ at 5.888 keV with probability 0.162 and Mn $K_{\alpha 2}$ at 5.899 keV with probability 0.6; the line centroid we use in this analysis, at 5.8988 keV, corresponds to the main component and the value used in the previous CTI analysis.

²The mask we use was derived from the illumination pattern of the calibration source for the Mn $K\alpha$ line, which may not be optimal for the Cu $K\alpha$, especially for the edge CCDs.

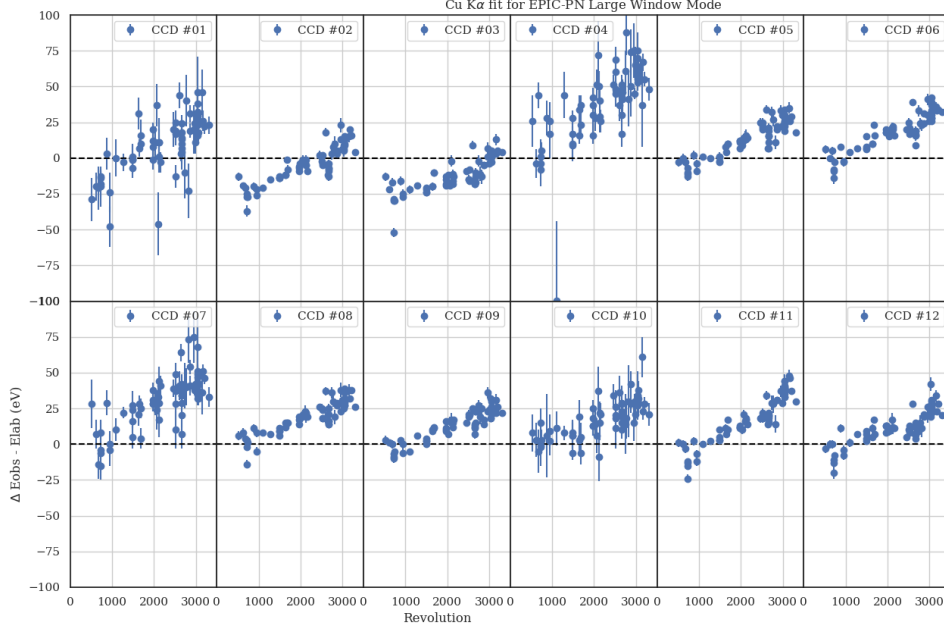


Figure 2: The difference in eV between the observed Cu $K\alpha$ line energy and the expected 8.04 keV for all 69 PN observations in Large Window mode. All observations, were processed with EPN_CTI_0048.CCF and `epchain withctlongterm=Y`.

3. For the single and double events analysis (see Sec. 3.5) we change (`PATTERN==0`) with the respective pattern selection: all doubles (`PATTERN` in `[1,4]`) or with the separate double pattern: (`PATTERN==X`), where X is from 1 to 4.
4. We fit a simple two-component model (Gaussian line + linear continuum) limiting the spectral energy range in [7-9] keV. The σ of the Gaussian line is only allowed to be within [40,250] eV. The fit is performed with a python package `lmfit`. An example of the fit for one OBS_ID is shown in Appendix C.

For the Cu $K\alpha$ analysis we use all available PN-LW observations with exposure time greater than 80 ksec.

3.3 Results using the current long-term CTI correction

The difference between the best-fit line centre and the expected energy for Cu $K\alpha$ using spectra produced with the current calibration files (EPN_CTI_0047.CCF and EPN_CTI_0048.CCF), is shown in Figure 2. We see a clear systematic trend with differences in recent epoch as high as 50 eV. Note that the Cu $K\alpha$ line is quite faint in some of the CCDs, most notably in CCD#4 (where the boresight is). The error bars reflect the faintness of the line.

The results show that the current long-term CTI correction, derived from Full Frame mode observations is not appropriate for Large Window mode for energies near 8 keV. By XMM-SAS implementation, the correction for PN-LW at energies greater than 5.8988 keV is the same as the LTCTI at 5.8988 keV (i.e. constant extrapolation). As we show in the previous subsection, we don't have enough good quality data to derive an updated correction at 5.8988 keV, therefore we proceed with the steps necessary to update the calibration file with a proper correction using only the Cu $K\alpha$ line.

3.4 Deriving the new long-term CTI correction

To derive the LTCTI for PN-LW we reprocess all observations, switching off the long-term CTI correction during the `epchain` steps with `withctlongterm=N`. And we perform exactly the same

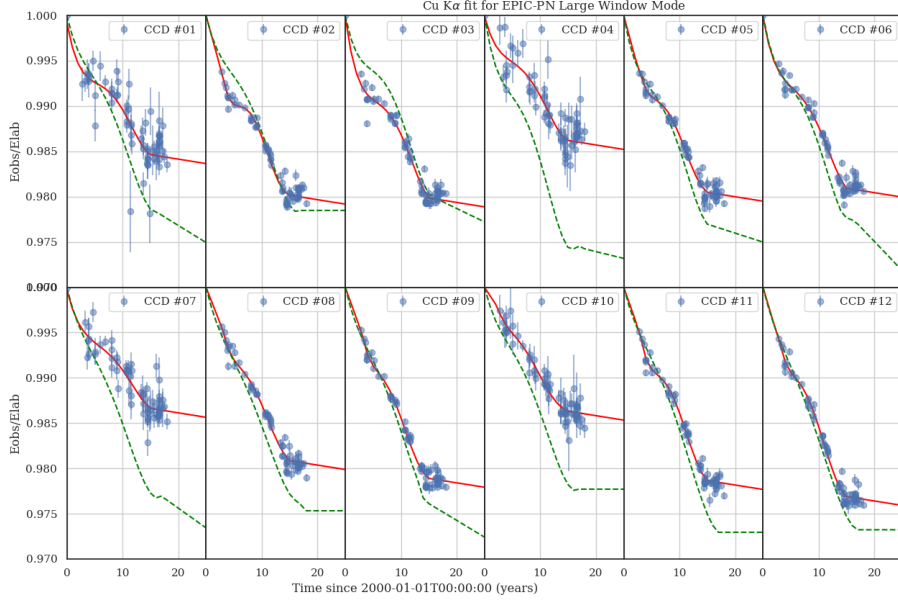


Figure 3: The ratio E_{obs}/E_{lab} of the Cu $K\alpha$ line energy as a function of time in years since 2000-01-01T00:00:00 for all 69 PN observations in Large Window mode. Each panel is for a particular CCD. All observations, were processed with `EPN_CTI_0048.CCF` and `epchain withctilongterm=N`. The green dashed curve is the current correction derived using Full Frame mode observations, the red curve is the proposed update.

steps as explained in Sec. 3.2 and extract non-CTI corrected spectra and fit the lines.

Once we have all the line centroid measurements (and their uncertainties) we can link the observed and measured line energies with the LTCTI:

$$E_{obs} = E_{lab} \times \text{LTCTI}(t, E_{ref}, \text{RAWY}), \quad (1)$$

where E_{obs} is the measured line centroid, E_{lab} is the laboratory line energy 8.04 keV of the Cu $K\alpha$ and $E_{ref} = E_{lab}$ is the reference energy for which we will derive the LTCTI. In the case of the instrumental Cu $K\alpha$ line we do not need any redshift correction for the line energy, so $E'_{lab} = E_{lab}$.

The results without the long-term CTI are shown in Fig. 3. We fit polynomials of 5th order for all CCDs except CCD#1, 4 or 7 where we select a polynomial of 4th order: these CCDs are visibly noisier than the rest and the higher order polynomials were overfitting the data. The extrapolation up to $t = 25$ was done in a way that $\text{LTCTI}(t = 25) = 0.999 \times \text{LTCTI}(t = 15)$ and linear function between those two points. This is somewhat an arbitrary choice and there are different alternatives, like keeping the LTCTI constant for the extrapolation. As we do expect some long-term effects for the CTI, then the linear decrease is preferable, although it is difficult to predict the rate of decrease.

We also set a linear extrapolation for LTCTI from the very first data point (at $t = 2.78$ years) to the initial point with $\text{LTCTI}(t = 0) = 1$.

The XMM-SAS implementation requires that the long-term CTI is encoded with the function $g(t)$ in

$$\text{LTCTI}(t, E_{ref}, \text{RAWY}) = E_{obs}/E_{lab} = \left[\frac{1 - g(t)}{1 - a_0} \right]^{\text{RAWY}}, \quad (2)$$

where t is the time measured in years since 01-01-2000T00:00:00, RAWY is the raw coordinate of the detector y-axis (the readout direction), a_0 is the CTI at $t = 0$ and its value is measured at launch using the calibration source, and $g(t)$ is a suitable function calculated on a grid of times starting at 0 and going to 25 with a step of 1 year (see [4]); $E_{ref} = 8.04$ keV is the reference energy for the curve. The XMM-SAS expects $g(t)$ for a set of reference energies and on a preselected set of

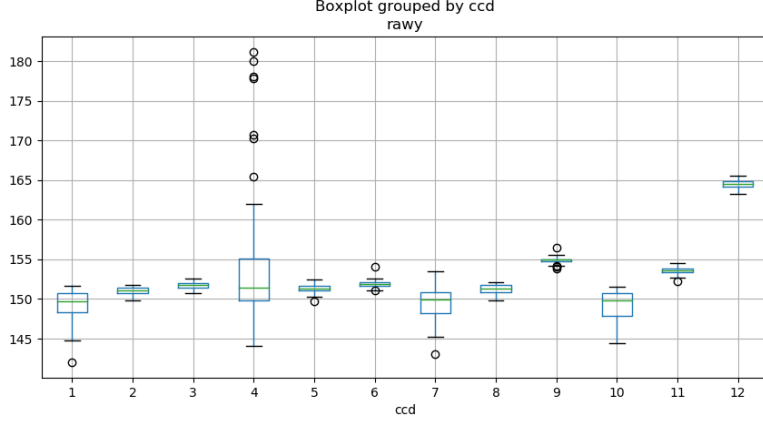


Figure 4: Box-and-whisker plot showing the distributions of the RAWY for the events within 8 ± 0.1 keV (around the peak of the Cu $K\alpha$ line). The box extends from quantile $Q1$ to $Q3$, the median ($Q2$) is indicated as a green horizontal line within the box, the whiskers extend to $1.5 \times (Q3 - Q1)$, the outliers are marked with circles.

times to be available in the `LONG_TERM_CTI` extension of the `EPN_CTI` calibration file. Consequently, we want to derive the best-fit $g(t)$ using the observed $LTCTI(t, E_{ref}, RAWY)$. So, rewriting Eq. 2 we obtain:

$$g(t) = 1 - (1 - a_0) \times LTCTI(t, E_{ref}, RAWY)^{1/RAWY}, \quad (3)$$

here a_0 and $RAWY$ are fixed for each source included in the analysis.

For the extracted spectra with CCD masks for PN-LW we have different mean $RAWY$ per CCD for the events within the energy range $[7, 9]$ keV. The $RAWY$ distributions are shown in a box-and-whisker plot in Fig. 4. We use the mean $RAWY$ for each CCD to derive the $g(t)$ curve (see Eq. 3).

The results after applying the new correction, by repeating the analysis as outlined in Section 3.2, using the newly generated `EPN_CTI_0049.CCF/EPN_CTI_0050.CCF`, are shown in Figure 5. We see a significant improvement of the derived line energies for Cu $K\alpha$ line for single events (pattern 0).

3.5 Correcting for the offset between events with different patterns

Figure 5 clearly indicates that the energies for double events (pattern 1 to 4) are offset from single ones, which we corrected for in the previous section. In order to derive the offset at the Cu $K\alpha$ line for each pattern and CCD, we generated spectra for each pattern of the double events and fit for the line centroid. The fit uncertainties are larger than those for single events or the combined doubles (see Fig. 6), but nevertheless we are able to derive the mean offset per CCD and per pattern and to update the `EPN_CTI_0049.CCF` extension `COMB_EVT_OFFSET` for PN-LW mode, adding a new energy shifts at energy 8.04 keV.

Note that the mean offsets, as derived with this processing, are relative to the already existing offsets at 5.8988 keV, because XMM-SAS `epevents` task assumes the same offset for all events at energies higher than 5.8988 keV (constant extrapolation for the offset).

The updated patterns 1 to 4 offsets for all 12 CCDs at the three energy points in `COMB_EVT_OFFSET`: at 1.486 keV (Al $K\alpha$ line), at 5.8988 keV (Mn $K\alpha$) and the new energy shift at 8.04 keV (Cu $K\alpha$) are shown in Fig. 7. Note that the two energy shifts at 1.486 and 5.8988 keV are derived from Full Frame mode observations (see [6]).

The final results with the newly implemented $LTCTI$ for PN-LW at 8.04 keV for single events (pattern zero) and with the implemented energy shift for double events (patterns 1 to 4) are shown in Fig. 8.

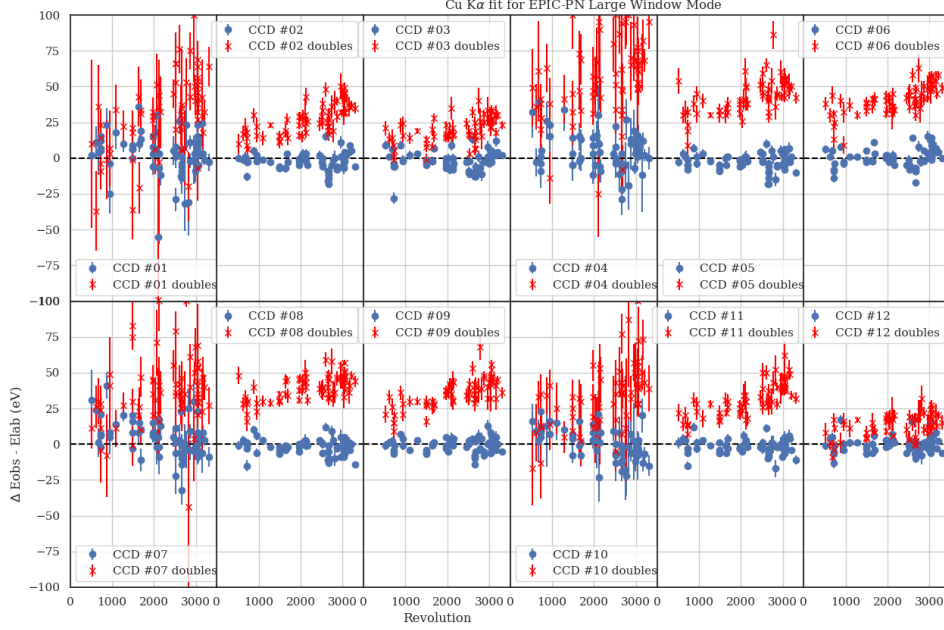


Figure 5: The results on the Cu $K\alpha$ after full reprocessing with EPN_CTI_0049.CCF. The y-axis is the difference of the best-fit line centroid and the expected line energy in eV. The blue symbols are for single events, while the red symbols are for doubles.

4 Test procedure

To test the updated calibration file we perform the same processing and analysis as outlined in Sec. 3.2 and using the same set of observation in PN-LW mode. The results of the tests are shown in Fig. 8 and the average energy offsets for the Cu $K\alpha$ line are presented in Table 1.

After applying the newly derived long-term CTI at 8.04 keV on the CalClosed and AGN observations we see a marginal improvement (~ 10 eV) closer to zero difference) to the offsets at 6.4 keV (see Fig. 1).

5 Scientific Impact and Estimated Quality

For observations in PN-LW the new long-term CTI correction should provide improved energy scale for spectral features at around 8 keV and will minimise the energy offset for single and double events. It is important to realise that the quality for CCD#4 (the boresight) is poor as the Cu $K\alpha$ fluorescent line only comes from a small region of the CCD. Similarly, the line is quite faint in CCDs 1, 7 and 10 too and consequently the results are with large uncertainties.

6 Expected Updates

The current correction does not update the long-term CTI at 5.8988 keV as there are not enough CC observations. A new PN-LW mode CalClosed observation is definitely needed in order to update the correction. The exposure time should be adjusted to provide enough signal-to-noise for the Mn $K\alpha$ line. Any change to the LTCTI at 5.8988 keV will likely require a new derivation for the currently implemented correction at Cu $K\alpha$ line at 8.04 keV and also the pattern shifts.

As the Iron-55 source is exponentially decaying, the Mn $K\alpha$ line is becoming too weak with not enough signal-to-noise to allow an analysis of the offsets for the different patterns. Therefore we do not expect any update to the COMB_EVT_OFFSET table at 5.8988 keV.

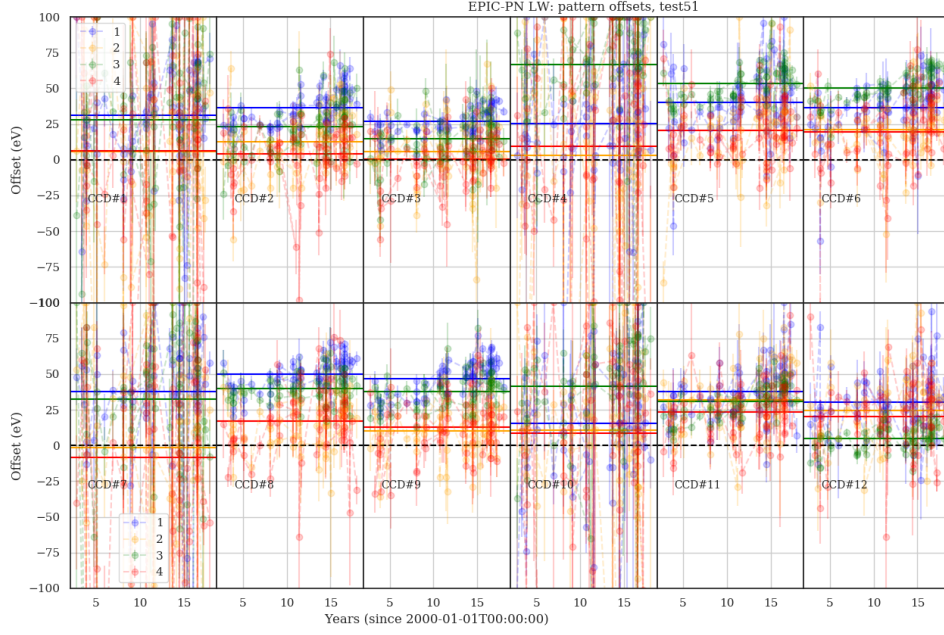


Figure 6: The results on the Cu $K\alpha$ centre offset for patterns 1 (blue), 2 (orange), 3 (green) and 4 (red). The horizontal lines are the derived mean values of the offset at 8.04 keV for each pattern. We use those to update the COMB_EVT_OFFSET extension in EPN_CTI_0049.CCF calibration file.

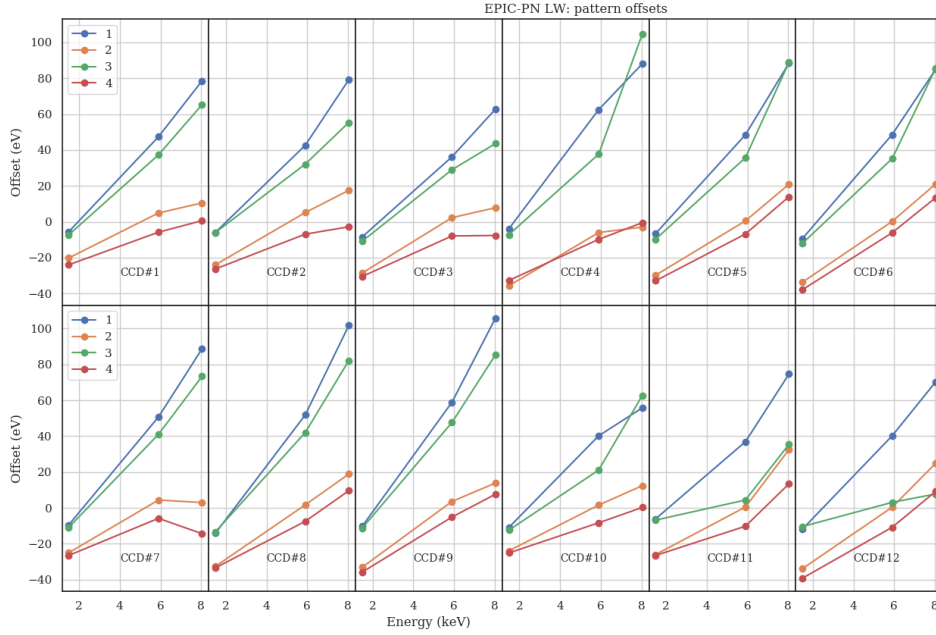


Figure 7: The updated energy shifts per CCD and per pattern as implemented in the COMB_EVT_OFFSET extension in EPN_CTI_0049.CCF calibration file. The two points at 1.486 and 5.8988 keV (Al and Mn $K\alpha$ lines) are derived from PN Full Frame mode observations. The point at 8.04 keV is the Cu $K\alpha$ line results from this study.

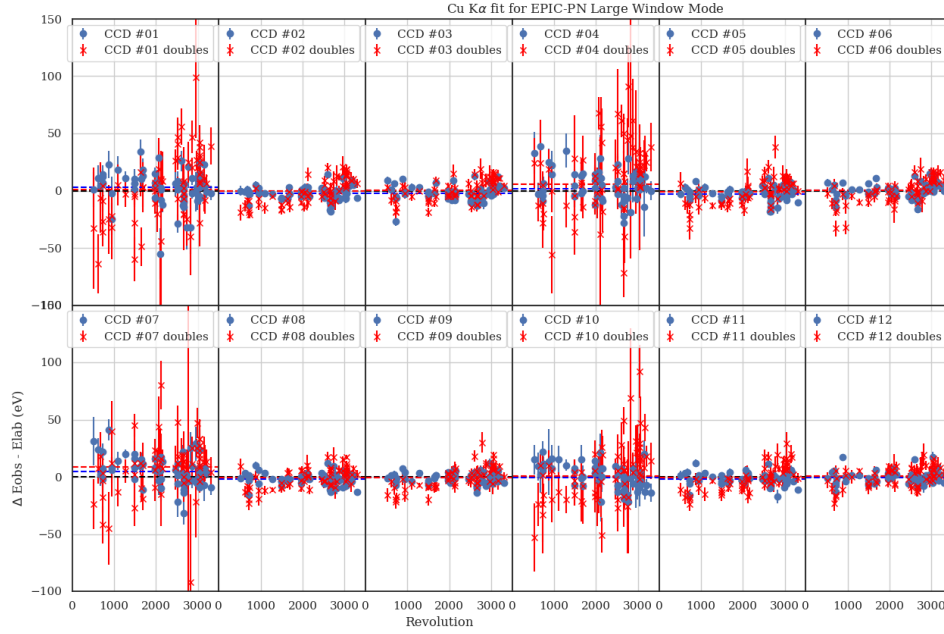


Figure 8: Final results for the Cu $K\alpha$ energy scale after implementing the LTCTI correction and the double pattern events offsets. Blue points: single events, red 'x': double events.

Table 1: The Cu $K\alpha$ best-fit line centre offset from 8.04 keV for single and double events, after processing with the updated calibration file. The results correspond to the data in Fig. 8.

CCD	Single events Mean \pm st.dev. (eV)	Double events Mean \pm st.dev. (eV)	CCD#	Single events Mean \pm st.dev. (eV)	Double events Mean \pm st.dev. (eV)
1	2.9 ± 14.7	0.8 ± 33.2	7	4.4 ± 12.5	8.4 ± 23.5
2	-2.6 ± 6.0	-0.6 ± 11.0	8	-2.2 ± 5.3	-0.9 ± 8.6
3	-2.0 ± 7.0	0.6 ± 9.0	9	-0.8 ± 4.7	-0.8 ± 9.9
4	1.8 ± 27.7	5.6 ± 45.9	10	-0.3 ± 10.2	0.6 ± 34.0
5	-2.7 ± 5.5	-0.8 ± 11.6	11	-1.9 ± 5.0	-0.9 ± 11.2
6	0.0 ± 6.2	0.2 ± 10.5	12	-0.4 ± 5.4	0.6 ± 8.3

7 Caveats

- **Long-term CTI or gain effect?**

The updated long-term CTI correction for the EPIC-pn Large Window mode is empirical. It is assumed that the observed systematic increase of the energy of the fitted line centres with time is due to a long-term CTI effect on the detectors and hence the deviation is modelled in such a way. The systematic shift to higher energies, however, could also be due in part to a gain effect caused by the quiescent background variations with time, although their influence at 8 keV is probably insignificant.

- **Contaminating out-of-time frame-store events.**

In both EPIC-pn window modes, the parts of the CCDs that are not read out are still exposed to the incoming X-rays, either from the sky or from the internal calibration source. When the selected window of the CCD is prepared for read out, it passes through the unexposed CCD area and into the frame-store for reading. The frame-store area is shielded from external X-ray photons. During this short transit, X-ray photons falling on the unexposed part of the chip will be superimposed on the actual observation – these are the so called out-of-time (OOT) events. The OOT fraction is usually much less than 10%. This effect is also present in observations of the calibration source and any fluorescent emission falling on the chips, it is illustrated in great details in [1].

Out-of-time events are expected in PN-LW observations of the Cu K α line. Only half of the CCDs are read out in PN-LW mode. The OOT events coming from RAWY < 100 but are assigned to RAWY > 100, hence Cu K α photons from the frame-store area will be “scattered” to higher energies. This effect will effectively lead to broadening of the line but the peak should be unbiased, if we assume an OOT fraction of $\lesssim 10\%$.

- **PN-LW correction at $E \sim 6$ keV.**

The updated long-term CTI correction at 8 keV improves a little bit but does not fix the energy offsets at ~ 6 keV (see Fig. 1). The corrected Cu K α line centres for the boresight CCD are with large uncertainties (see Fig. 8, CCD#4), nevertheless a possible systematic offset of ~ 30 eV at energies $\lesssim 6$ keV should be considered for sky sources at the boresight.

- **PN-LW double vs single events energy shift.**

The implemented energy shift of double events (PATTERN in [1:4]) at 8 keV should in principle improve the spectral resolution at these energies for double events, as well as for selection of both single and double events.

References

- [1] Freyberg, M., 2006, [EPIC-pn large window mode fast-shift CTI correction](#), XMM-Newton Calibration meeting, MPE
- [2] Jones, E., Oliphant, E., Peterson, P., et al. SciPy: Open Source Scientific Tools for Python, 2001-, <http://www.scipy.org/>.
- [3] Sanders, J. & Dennerl, K., 2017, [Calibrating the EPIC-pn energy scale with the Cu fluorescent line](#), XMM-Newton Calibration meeting, Garching
- [4] Smith, M.J.S, Guainazzi, M., Cappi, M., 2010, [XMM-CCF-REL-271](#), EPIC-pn Long-Term CTI
- [5] Smith, M.J.S, Guainazzi, M., Marinucci, A., 2013, [XMM-CCF-REL-300](#), EPIC-pn Long-Term CTI
- [6] Smith, M.J.S, Stuhlinger, M., Saxton, R.D., Freyberg, M.J., 2014, [XMM-CCF-REL-323](#), EPIC-pn Long-Term CTI and Energy Scale
- [7] Smith, M.J.S, 2016, [XMM-CCF-REL-336](#), EPIC-pn Long-Term CTI
- [8] Smith, M.J.S, Dennerl, K. & Freyberg, M.J., 2018, [XMM-CCF-REL-358](#), EPIC-pn Energy Scale: Long-Term CTI and Quiescent Background Gain Correction.
- [9] Valtchanov, I., Smith, M.J.S, Schartel, N., 2019, [XMM-CCF-REL-366](#), EPIC-pn Energy Scale for Small Window mode.

Appendix

A PN-LW CalClosed and AGN observations.

Table 2: Listing of the PN-LW CalClosed observations included in the analysis and the Mn K α fit at the boresight (indicated with CCD#4.2) using the current calibration files (v48). These correspond to the data points shown in Fig. 1. ΔE (and its error) is the difference in eV of the best-fit line energy and the expected 5.8988 keV.

OBS_ID	Expo	Rev.	Δt [yr]	t_{expo} [ksec]	CCD	Line E [keV]	E_{err} [keV]	ΔE [eV]	ΔE_{err} [eV]	C-stat	χ_r^2	D.O.F
0094780201	S003	134	0.6682	16.2	4.2	5.8938	0.0016	-5.0	1.6	598.30	1.351	391
0041150201	S001	255	1.3296	7.0	4.2	5.8881	0.0027	-10.7	2.7	434.49	0.723	391
0157771001	S014	581	3.1126	31.6	4.2	5.9021	0.0017	3.3	1.7	649.22	1.526	391
0203720201	S020	885	4.7766	14.0	4.2	5.9031	0.0032	4.3	3.2	476.68	0.854	391
0727360201	S003	3274	17.8299	14.4	4.2	5.9193	0.0212	20.5	21.2	325.38	0.301	391

Table 3: Listing of the sky sources included in the PN-LW analysis. ΔE (and its error) is the difference in eV of the best-fit line energy and the rest-frame energy of Fe K α of 6.399/(1+z) keV.

OBS_ID	Expo	Rev.	Δt [yr]	t_{expo} [ksec]	Line E [keV]	E_{err} [keV]	ΔE [eV]	ΔE_{err} [eV]	C-stat	χ_r^2	D.O.F
ngc3227, $z = 0.00386$											
0400270101	S003	1279	6.9263	93.6	6.372	0.01	-2.4	10.0	852.4	1.0927	794
Tycho SNR, $z = 0.0$											
0412380401	S003	1773	9.6251	29.4	6.439	0.019	40.0	19.0	811.1	0.773	794
mkn1040, $z = 0.016338$											
0554990101	S001	1682	9.1281	66.5	6.313	0.019	16.9	19.0	852.1	1.1132	794
0760530201	S001	2871	15.6257	84.5	6.337	0.016	40.9	16.0	848.3	1.0999	794
mkn883, $z = 0.03787$											
0652550201	S013	1959	10.6422	25.8	6.192	0.035	26.5	35.0	876.4	0.8528	794
ngc5899, $z = 0.0088$											
0651850501	S003	2048	11.1277	18.2	6.37	0.041	26.8	41.0	832.0	1.4721	794
ngc526a, $z = 0.01897$											
0721730301	S003	2570	13.9822	48.5	6.314	0.021	34.1	21.0	831.7	1.1141	794
mkn915, $z = 0.024043$											
0744490401	S003	2744	14.9304	85.8	6.277	0.02	28.2	20.0	791.4	1.0723	794
ngc6814, $z = 0.005227$											
0764620101	S001	2991	16.2801	103.1	6.392	0.011	26.3	11.0	872.0	1.1303	794

B Cu $K\alpha$ spatial distribution in an PN-LW observation.

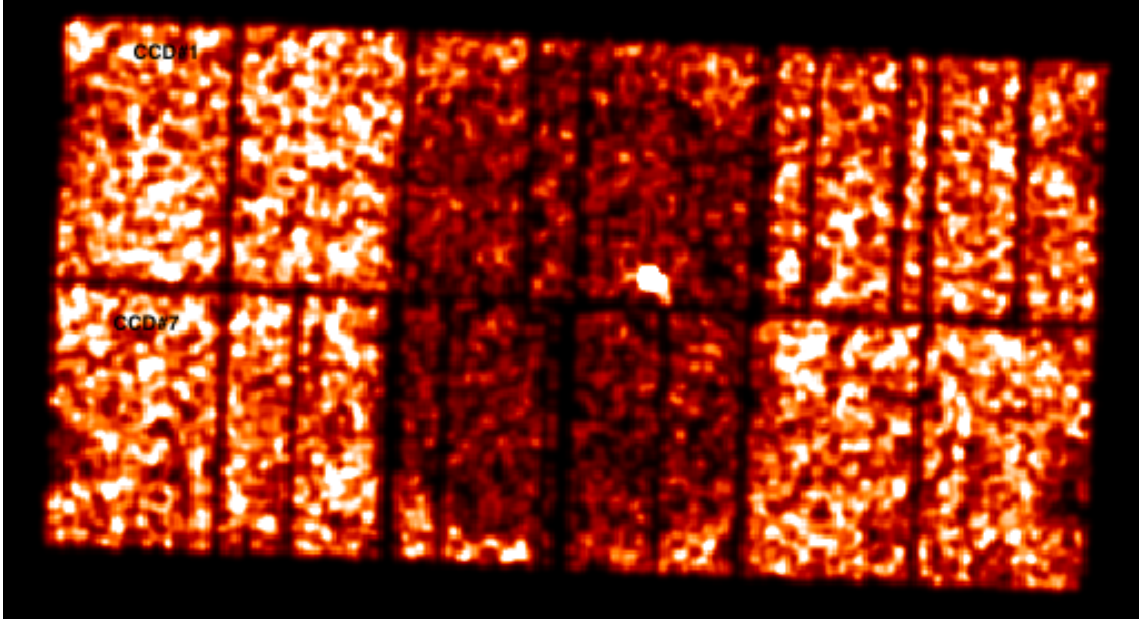


Figure 9: Cu $K\alpha$ spatial distribution. The image is made of all events with energies between 7.9 and 8.1 keV. For clarity, the distribution is smoothed with a Gaussian with FWHM of $15''$. There is a sky source indicating the boresight in CCD#4.

C Example fit for the Cu $K\alpha$ line in a PN-LW observation.

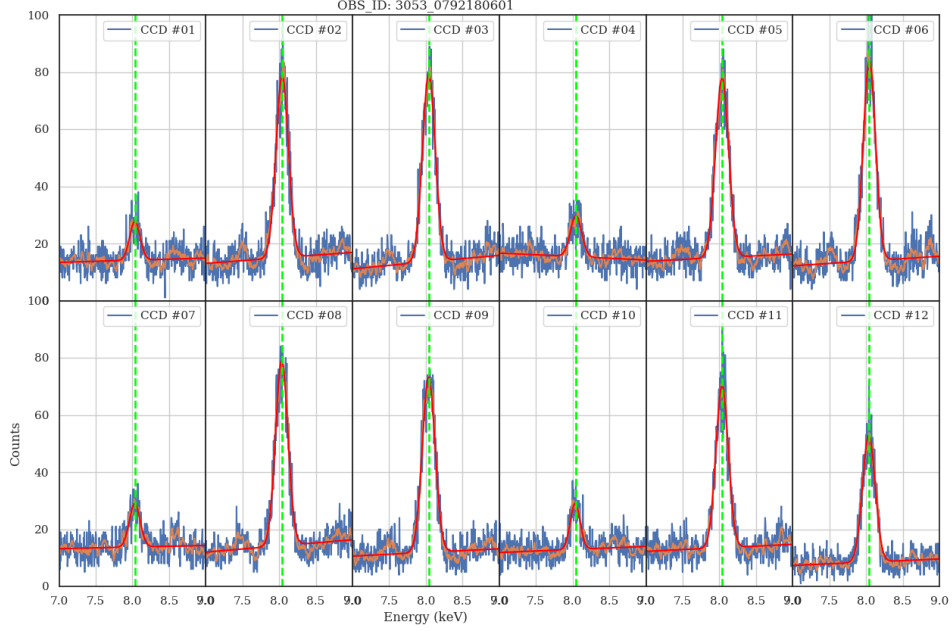


Figure 10: Cu $K\alpha$ fit results for single events (pattern=0) and per CCD, using the updated calibration file. The blue curves are the raw spectra in [7:9] keV, where we fit a model with a single Gaussian line and linear continuum. The red curve is the best-fit model, the orange curve is the smoothed spectrum (boxcar smoothing with 7 elements, i.e. ~ 35 eV smoothing length) only shown for reference, the fit was performed with the raw spectrum. The vertical green dashed line is the expected line centre (8.04 keV).

D XSPEC line fit plots for the Fe $K\alpha$ line

XSPEC output plots for all PN-LW observations listed in Tab. 3.

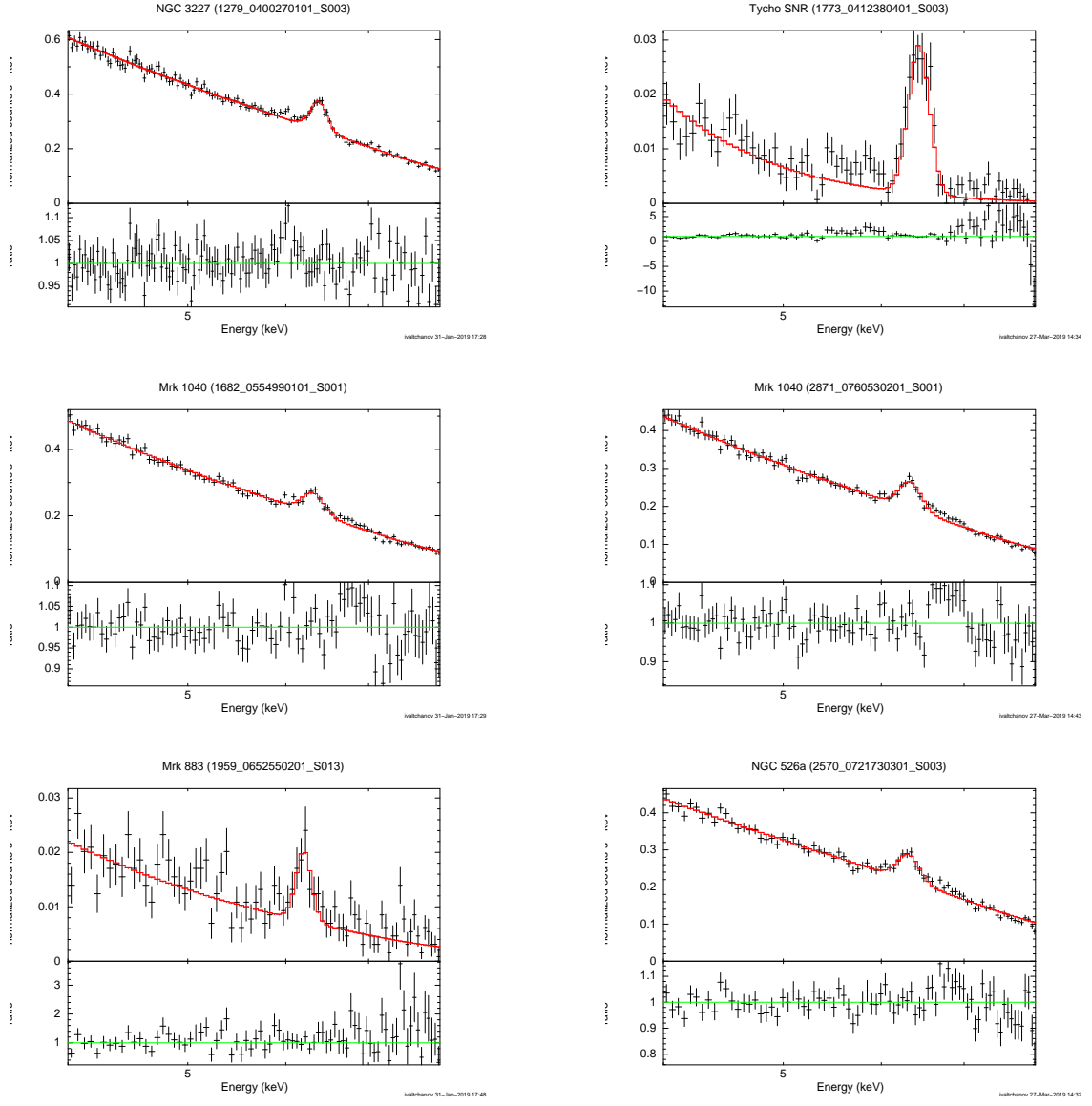


Figure 11: Fe $K\alpha$ fit results.

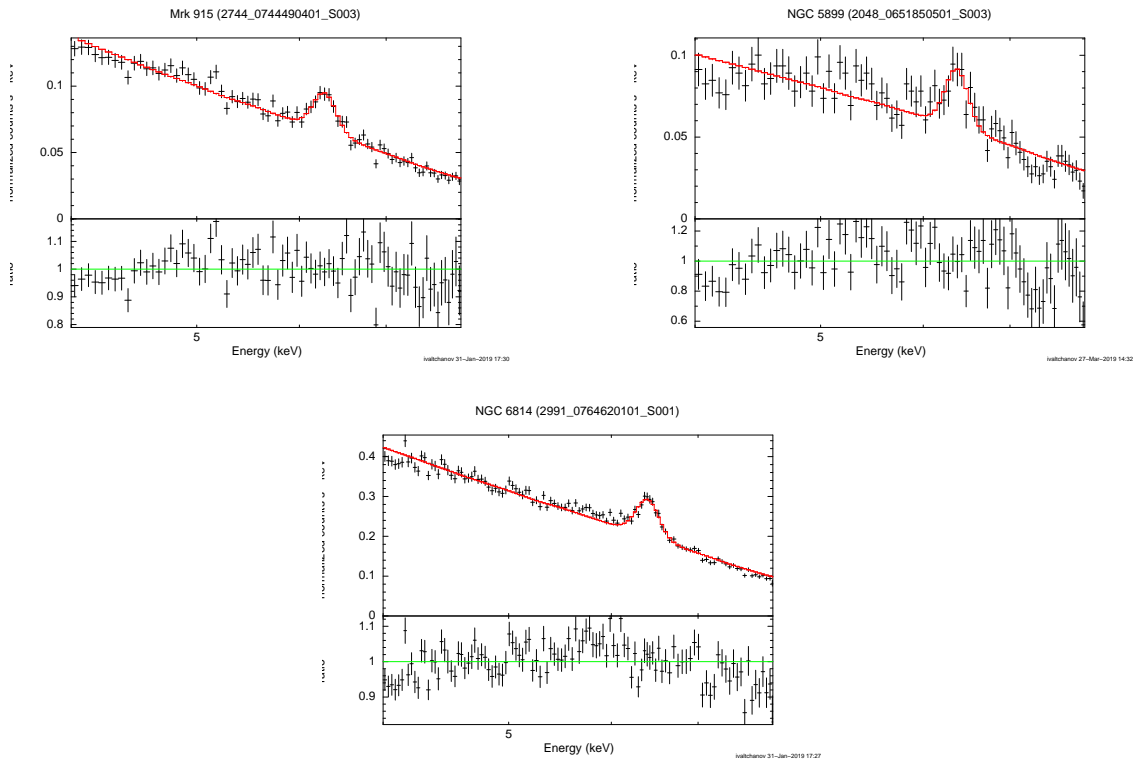


Figure 12: Fe K α fit results, continued.